

Water Resources Research

RESEARCH ARTICLE

10.1029/2020WR027989

Key Points:

- Volume of seasonal wetlands dominated by monsoon runoff is estimated for northeastern Bangladesh using remote sensing
- Storage in wetlands relative to the lowest observable level varies from $6.5 (\pm 0.4) \text{ km}^3$ at the start of the monsoon to $30.9 (\pm 2.0) \text{ km}^3$ when monsoon ends
- The gauge-satellite data approach can be used for global wetland and seasonal lake monitoring with the launch of the SWOT mission

Supporting Information:

- Supporting Information S1

Correspondence to:

F. Hossain,
fhossain@uw.edu

Citation:








Ahmad, S. K., Hossain, F., Pavelsky, T., Parkins, G. M., Yelton, S., Rodgers, M., et al. (2020). Understanding volumetric water storage in monsoonal wetlands of northeastern Bangladesh. *Water Resources Research*, 56, e2020WR027989. <https://doi.org/10.1029/2020WR027989>

Received 21 MAY 2020

Accepted 31 OCT 2020

Accepted article online 5 NOV 2020

Understanding Volumetric Water Storage in Monsoonal Wetlands of Northeastern Bangladesh

Shahryar Khaliq Ahmad¹ , Faisal Hossain¹ , Tamlin Pavelsky² , Grant M. Parkins^{2,3}, Sarah Yelton^{2,3} , Megan Rodgers^{2,3}, Sarina Little² , Debolina Haldar⁴, Sheikh Ghafoor⁴ , Raihanul Haque Khan⁵, Nazmul Ahsan Shawn⁵, Aminul Haque⁵, and Robin Kumar Biswas⁶ 

¹Civil and Environmental Engineering, University of Washington, Seattle, WA, USA, ²Department of Geological Sciences, University of North Carolina at Chapel Hill, Chapel Hill, NC, USA, ³Institute for the Environment, University of North Carolina at Chapel Hill, Chapel Hill, NC, USA, ⁴Department of Computer Science, Tennessee Technological University, Cookeville, TN, USA, ⁵HMRC Limited, Dhaka, Bangladesh, ⁶Bangladesh Water Development Board, Dhaka, Bangladesh

Abstract The volume of water stored in seasonal wetlands is a fundamental but difficult to measure variable for developing a physical understanding of wetland behavior. For seasonal wetlands that are a major source of water for rice and fish production, this physical understanding is key to planning for water-food security and ecosystem services. This study quantified variations in volumetric storage for the numerous seasonal wetlands of northeastern Bangladesh, locally known as “haors.” These haors receive transboundary runoff from densely vegetated and mountainous terrain in India and face persistent monsoonal cloud cover as they become full. We estimated volumetric storage for 13 haors by using extensive remote sensing data on water surface extent and elevation that was complemented with citizen-contributed gauge data. Assuming a trapezoidal bathymetry, an area-volume relationship was developed for selected haors. This relationship was assumed to be valid for extrapolating volumetric estimations over all the haors in the region. Results suggested that as haors get filled with the onset of monsoon rains, total estimated storage relative to the lowest observable level varied from $6.5 (\pm 0.4) \text{ km}^3$ in May to $30.9 (\pm 2.0) \text{ km}^3$ in July (peak of monsoon). Choosing a rectangular bathymetry can lead to 47% higher estimates compared to trapezoidal cross section. Estimating this intra-annual/interannual increase in storage is important for the region to plan water management policies that balance the human and ecosystem needs. Our analytical approach has potential for application to wetlands worldwide in light of the upcoming Surface Water and Ocean Topography (SWOT) mission.

1. Introduction

Wetlands, among the world's most productive environments, are defined by U.S. Geological Survey as transitional areas between permanently flooded deep-water environments and well-drained uplands. Wetlands serve as cradles of biological diversity and provide water and productivity for countless plants and animal species to thrive (Amezaga et al., 2002; Parish & Looi, 1999). In addition to supporting groundwater recharge, flood control and ecosystems, wetlands also act as natural water purifiers and enhance groundwater quality (Bullock & Acreman, 2003; Kamal et al., 2018; Kaplan & Avdan, 2018; Mitsch & Gosselink, 2000; Ogawa & Male, 1986).

The seasonal wetlands in northeastern Bangladesh, locally termed as “haors,” are of specific significance as they are a source of rich biodiversity and livelihood for about 20 million inhabitants. These water bodies exhibit strong seasonality in storage that peaks during the Monsoon months of August–September. A productive fisheries economy is created when the low-elevation land is inundated with transboundary runoff from Indian mountains (Kamruzzaman & Shaw, 2018). As flood waters recede during the dry season (November to April), water levels drop to expose the rich alluvial soils around the haor margins. This soil is optimally primed for rice cultivation (Bennett et al., 1995). Thus, the haor region experiences extensive dry season rice cultivation from November to April that provide nearly one fourth of total rice production for Bangladesh. The haors are also strongly connected to groundwater aquifers by acting as recharge points. With rising concerns regarding impacts of changes in climate and land use on hydrology in South Asia (Dwarakish & Ganasri, 2015; Turner & Annamalai, 2012; Wijesekara et al., 2012), accurate mapping and monitoring of the haors in a feasible and cost-effective way is now timely.

Efforts to monitor wetlands and lakes (hereafter used interchangeably) have generally used satellite remote sensing due to limited availability of in situ gauges, inaccessibility of wetlands and slow dissemination of ground-based data. Optical and synthetic aperture radar (SAR) remote sensing data have been used extensively to detect and map the areal extent of surface waters (Huang et al., 2018; Kaplan & Avdan, 2018), including those in Bangladesh (Dewan et al., 2007; Hossain, 2013). Popular optical satellite missions used for surface water detection include Landsat (Chen et al., 2014; Gao et al., 2016; Pardo-Pascual et al., 2012), Moderate Resolution Imaging Spectroradiometer (MODIS) onboard the Terra and Aqua satellites (Brakenridge & Anderson, 2006; Chen et al., 2013; Peng et al., 2005), and Visible Infrared Imaging Radiometer Suite onboard Suomi National Polar-orbiting Partnership (Suomi NPP-VIIRS) (Huang et al., 2015). The European Space Agency's Sentinel-2 mission also provides relatively high-resolution multi-spectral imagery which can be used to map surface water (Du et al., 2016; Yang, Zhao, et al., 2017). However, optical sensors are unable to penetrate clouds and thus are not suitable for use in South Asian environments during the monsoon season. In contrast, SAR data such as that from the Sentinel-1 satellite overcomes the cloud interference issue and works during both the day and night for water detection (Shen et al., 2019; White et al., 2015).

Applications of current optical and microwave imagers to the study of lakes are limited, however, as they can only estimate the spatial extent, or area, of the water bodies. On the other hand, satellite radar altimeters, originally developed for oceanographic studies (Brown & Cheney, 1983), can provide estimates of lake water surface elevations by measuring the two-way travel time of radar pulses reflected from the water surface (Birkett & Beckley, 2010). Radar altimetry missions in service include Cryosat-2, HY-2, SARAL/Altika, Jason-3, and Sentinel-3A and Sentinel-3B (Wang, 2019). The uncertainty of present altimetry missions ranges within a few centimeters for bigger lakes but increases to tens of centimeters for rivers and smaller lakes (Crétaux et al., 2018; Villadsen et al., 2016). Their long repeat cycle (minimum being 10 days) makes the altimeter susceptible to miss key hydrological events (Sulistioadi et al., 2015). Furthermore, the limited spatial coverage of nadir-pointing altimeters allows monitoring of elevation for only a small set of wetlands. This is where the power of citizen science can complement satellite remote sensing to provide a more complete view of wetland dynamics. Recent projects have demonstrated the potential for citizen scientists to accurately monitor surface water bodies (Lowry & Feinen, 2013; Lowry et al., 2019; Strobl et al., 2019). One such project, Lake Observations by Citizen Scientists & Satellites (LOCSS), is designed to harness citizen science to acquire water elevation for lakes in multiple countries (<https://www.locss.org/>). Water surface elevations are measured by volunteers reading simple lake gauges that are then shared with the project via text message or other means. Such citizen-contributed lake height data provide a viable alternative to a traditional ground-based system that requires a larger institutional capacity for maintenance and monitoring, when automated gauges are absent or sparsely distributed.

While information on wetland areal extent and water surface elevation is possible to obtain from the satellite missions and citizen science data, the key unknown for developing a process-based understanding of haor hydrology is the volume of water stored in these seasonal water bodies. Volume is a significant water balance indicator and has implications for water-food security and ecosystem services in northeastern Bangladesh. Knowing the volumetric storage in the haor systems can help plan for uncertainty in available water for water security (Gaupp et al., 2015). A few studies have derived changes in lake volume using simultaneous analysis of area and water level (Chipman, 2019; Smith & Pavelsky, 2009). Crétaux et al. (2016) used successive measurements of area and elevation to determine volume variation assuming a pyramidal bathymetry of lakes in Tibetan Plateau. Tong et al. (2016) derived time series of water volume by using a combination of multimission altimetry and remotely sensed images for Lake Victoria. Studies have also used digital elevation models (DEM) along with remote sensing imagery for the same purpose (Yang, Zhu, et al., 2017). Finally, changes in water storage in large lakes have also been inferred from interferometric radar (InSAR) measurements of the displacement of the surrounding terrain (Zhao et al., 2016) and from satellite gravimetry missions such as the Gravity Recovery and Climate Experiment (GRACE) (Ni et al., 2017).

Most of the studies on lake volume estimation have considered large lakes or wetlands and those specifically located in relatively dry and arid climates. Studies on seasonal wetlands are still limited due to scarcity of synchronous radar altimeter data, difficulty in acquiring high-resolution images of inundation extent and inconsistent ground data. A small artificial lake in France was studied by Baup et al. (2014) using altimetry and optical images, but consistent studies of volume variations in smaller water bodies from satellite imagery

remain scarce. The haors of Bangladesh are particularly challenging for space-based monitoring. They exhibit highly dynamic responses to a strong seasonal cycle under the tropical seasonal monsoon climate. The wetland surfaces usually host an abundance of dense vegetation, often forming a thick layer of free-floating plants obstructing the inundation beneath from being accurately mapped from space (Ahmad et al., 2019). The haors are spread over the basin of Northeast Bangladesh (referred to as the “haor basin” hereafter) in large numbers. As the basin’s hydrology is dominated by seasonal transboundary runoff, the haors often merge to form larger water bodies with the onset of monsoon season. The highly transient nature of their maximum spatial extent and depth presents another formidable challenge in their monitoring and mapping and impedes effective management of water resources.

The present study addresses these challenges using the state-of-the-art advancements in satellite remote sensing while harnessing the power of citizen scientists in collecting ground-based information on water heights. This study aims to determine the value of using citizen science data and remote sensing on seasonal water bodies to understand the total volumetric storage and volume change in the monsoonal and transboundary runoff-dominated region of Northeastern Bangladesh.

In an effort to estimate volume storage across all the haors in the basin, we incorporated a variety of satellite products at different wavelengths to obtain the spatial extent (using microwave satellite products) and vertical depth (using radar altimetry) for 13 haors. We then estimated two variables of hydrologic significance for the region, (i) volume of water stored by the haor relative to its lowest observable level and (ii) volume of water moving through the haor system in a water year. Because only a limited set of haors can be studied using current satellite missions and citizen science data, an algorithm was developed to delineate each haor individually and obtain their representative areas from satellite imagery. An area versus volume relationship was established over the selected 13 haors. This relationship, assumed to hold true for all haors of the basin, was then used to provide a statistical estimate of the cumulative volume storage and volume change across the entire haor basin. The computational and data storage constraints were addressed in the study by using the Google Earth Engine (GEE) cloud-based computing platform (Gorelick et al., 2017). Thus, our study was able to quantify a previously elusive but fundamental insight on the volumetric dynamics of the haors that is critical for planning of water-food security, ecosystem services, and adapting to changes from human impacts and climate.

The rest of the paper is organized as follows. In section 2, we describe the selected sites for satellite- and citizen science-based analysis and necessary data sets. This is followed by a description of the methodology in section 3. The results on estimates of volumetric variables for the haor basin are presented in section 4, followed by discussion and concluding remarks in section 5.

2. Study Sites and Data Sets

2.1. Selected Lakes

The extent of the haor basin that is the focus of this study is shown in Figure 1. Within the basin, specific sites were selected for the purpose of establishing our volume estimation approach. Under the LOCSS project, two lakes in the haor basin, Korchar and Dekhar haors, are currently monitored for water levels by citizen scientists (see <https://www.locss.org/region/bangladesh>). As data over only two haors and a single water year of 2019 have been acquired until now, additional sites are naturally needed for establishing a reliable volume estimation approach. This was made possible by the use of satellite radar altimeters. Haors located along the altimeter passes (described in section 2.2) were chosen as virtual stations for water level monitoring. The characteristics and sources of water levels for the selected haors and the period of availability of altimeter data are summarized in Table 1. Figure 1 shows the locations of haors and altimeter paths. Annual mean area of selected haors is 390 km² covering 6.6% of all haors in the basin with an area of 5,900 km². The areas of selected haors cover a reasonable range of all the existing haor areas, albeit very small haors (<1 km²) could not be considered due to limitations in monitoring them using altimetry or LOCSS (see Figure S1 in the supporting information).

2.2. Data Sources

The primary source for mapping lake surface area was C-band synthetic aperture radar ground-range detected (SAR GRD) microwave satellite imagery from Sentinel-1A with a spatial resolution of 10 m and

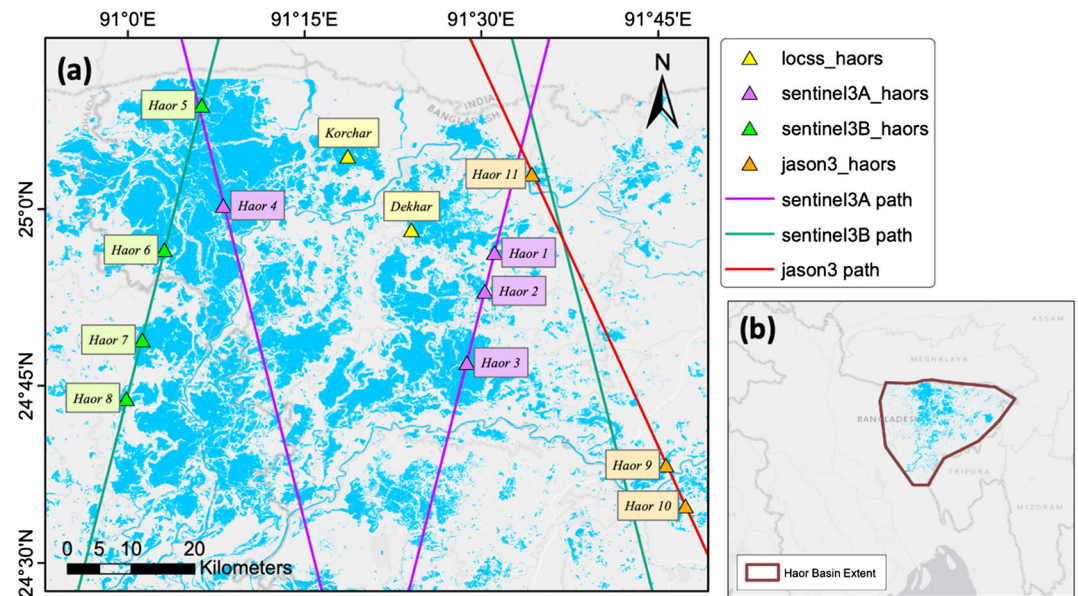


Figure 1. (a) Haors selected over the northeast region of Bangladesh for the volume estimation analysis, also showing the different altimeter passes used for elevation data in addition to that from citizen science. (b) Footprint of the selected extent for haor basin.

6-day revisit period. A SAR product was used due to its ability to penetrate clouds and, in some cases, vegetation, as required in the tropical monsoonal climate of Bangladesh. The images were retrieved for a 4-year time period spanning 2016 to 2019. For water depths, in addition to LOCSS data, two altimeter missions, Jason-3 and Sentinel-3 were used. The Jason-3 nadir altimeter is the follow-on mission to TOPEX/Poseidon (T/P) and Jason-1/Jason-2, distributed by CNES (Centre National d'Études Spatiales) AVISO (Archiving, Validation and Interpretation of Satellite Oceanographic Data). The 20-Hz Geophysical Data Record (GDR) of the Jason-3 altimeter has a repeat cycle of 10 days and passes over the haor basin to provide potential virtual stations. The Ku-band data sets from cycle 0 to cycle 142 (dated 12 February 2016 to 27 December 2019) were downloaded and processed to extract water elevations.

The Sentinel-3 satellite mission, managed by the European Space Agency (ESA) and the European Organization for the Exploitation of Meteorological Satellites (EUMETSAT), has a repeat cycle of 27 days.

The SAR Altimeter (SRAL) instrument onboard Sentinel-3 is a dual-frequency (Ku- and C-band) nadir-looking radar altimeter providing estimates of sea surface height and surface wind speed at the global scale. The SRAL Non-Time-Critical (NTC) Land Level 2 products were selected for processing. Sentinel-3A data from 12 March 2016 to 24 December 2019 (Cycles 1–52) for Relative Orbit Numbers 96 and 375, and Sentinel-3B data from 27 December 2018 to 13 Dec 2019 (Cycles 20–33) for Relative Orbit Numbers 154 and 375 were used in the study. The data were downloaded through Copernicus Online Data Access (<https://scihub.copernicus.eu/dhus/>). Enhanced measurement data for the SRAL product, which contains necessary parameters to reprocess the data (Yang & Zhang, 2019), were used for processing the water levels.

To assess the quality of haor classification and volume storage estimates, we used high-resolution imagery in visible and NIR bands from Planet (formerly known as Planet Labs) (Planet Team, 2017). The platform has a constellation of more than 170 active CubeSats, that provides daily global imaging in the visible and NIR bands at 3-m resolution (Planet Imagery Product Specification, 2019). The Level 3A PlanetScope Ortho Tile Product from the Planet Explorer imagery exploration tool was used

Table 1
Details for the Selected 13 Haors (11 on Altimeter Path and Two From LOCSS Observations) and Their Extents for Volume Estimation Analysis

S. No.	Haor ID	Source of elevation	Time period	Maximum area (km ²)
1.	Haor 1	Sentinel-3A	2016–19	4.1
2.	Haor 2	Sentinel-3A	2016–19	14.6
3.	Haor 3	Sentinel-3A	2016–19	90.5
4.	Haor 4	Sentinel-3A	2016–19	100.8
5.	Haor 5	Sentinel-3B	2019	100.1
6.	Haor 6	Sentinel-3B	2019	96.3
7.	Haor 7	Sentinel-3B	2019	97.6
8.	Haor 8	Sentinel-3B	2019	35.7
9.	Haor 9	Jason-3	2016–19	54.9
10.	Haor 10	Jason-3	2016–19	95.1
11.	Haor 11	Jason-3	2016–19	18.5
12.	Korchar	LOCSS	2019 wy ^a	72.0
13.	Dekhar	LOCSS	2019 wy ^a	3.9

^aRefers to water year of 2019.

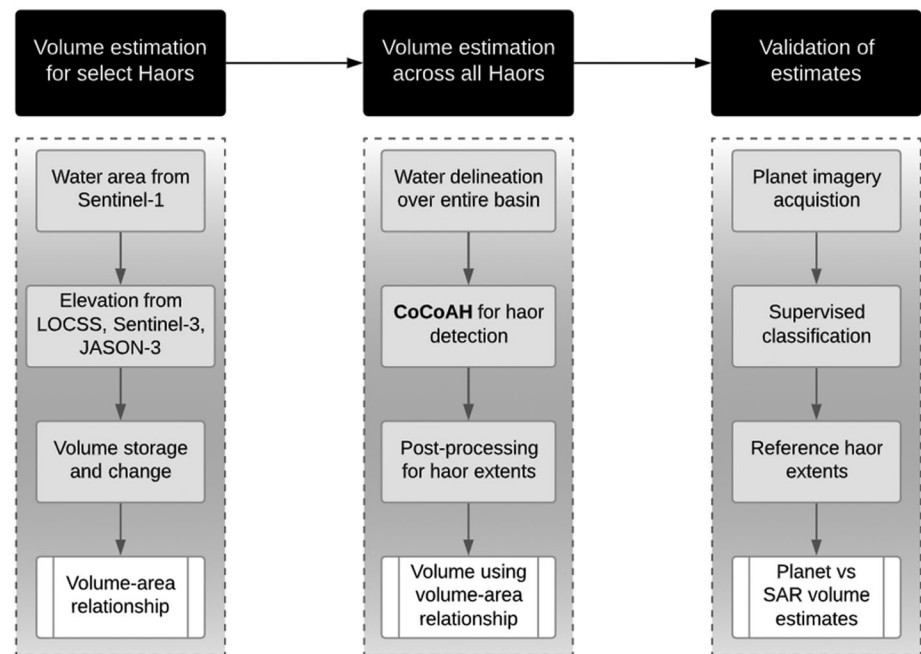


Figure 2. Overview of the methodology for volume estimation in the haor basin using LOCSS and remote sensing products.

for classifying the haors and estimating their volume storage. We have used the same data to validate inundation extent measurements as in a previous study over the same region (Ahmad et al., 2019).

The JavaScript API of the GEE platform was used for processing the Sentinel-1 SAR remote sensing product, which is available from the GEE data catalog. The volume estimation approach was developed and implemented using the MATLAB Image Processing Toolbox.

3. Methods

An overview of the methodology followed is shown in Figure 2. The haor basin's volumetric storage estimation consists of three key components—(i) deriving volume for haors using available data on area and elevation, (ii) estimating volume (storage and change) for all the haors across the basin, and (iii) comparison of results against high spatial resolution data. The following sections describe each component in detail.

3.1. Haor Volume Using LOCSS Data and Remote Sensing

Deriving haor volume requires simultaneous knowledge of two state variables: haor area and elevation. Microwave remote sensing was used to estimate the area, while LOCSS and satellite radar altimetry were employed to obtain the elevation of haors. Sections 3.1.1 and 3.1.2 provide details on the methodology for deriving these variables while section 3.1.3 outlines the procedure for validating volume estimates.

3.1.1. Haor Area

A water classification technique was applied to Sentinel 1 SAR GRD imagery at 10-m spatial resolution which relies on the low backscatter from smooth surfaces of water bodies. Co-polarized Sentinel-1 scenes with vertical (VV) transmitter-receiver polarization (vertical transmitted and vertical received) were selected from the GEE data catalog. The scenes in the catalog are multilooked, processed to remove thermal noise, radiometrically calibrated, orthorectified, and georeferenced. However, the quality of the radar product degrades with the signal dependent on granular interference, called “speckle.” Speckle is primarily caused by the phenomenon of interference of the returning wave at the transducer aperture. To reduce this interference, a focal median filter with 30-m window (large enough to capture speckle) was applied to smooth the image. Median filters are shown to perform better than mean or Gaussian filters, in general, for high levels of speckle in SAR images (KlogoGriffith et al., 2013). The SAR look angle was bounded within 31.7° to 45.4° to

avoid coarse spatial resolution at lower angles and small signal-to-noise ratios at higher angles (Nagler et al., 2016). Water in the postprocessed image was then classified using backscatter-based thresholding. Pixel values with backscatter value less than a threshold of -13 dB were assigned the water class, as standing water exhibits levels of backscatter ranging from -24.3 to -12.6 dB (Liu, 2016). The algorithm is similar to that proposed by Ahmad et al. (2019) in their fusion approach, except no optical imagery could be used here due to high interference from clouds over the haor basin. The accuracy of water detection using the fusion approach was reported between 85.8% and 98.7%, and Kappa coefficient between 0.61 and 0.83 by Ahmad et al. (2019). Using this algorithm, an area time series was obtained for the selected haors to be later used for volume calculation (see Figure 7).

3.1.2. Haor Elevation

The elevation of haors was obtained using multiple sources. The LOCSS project has gathered citizen-contributed water height data over Korchar and Dekhar haors (see Figure 1) over a single water year (at the time of writing). Because a single water year does not provide enough data to derive a robust volume-area relationship, two radar altimeters, Jason-3 and Sentinel-3 were used to monitor additional haors. In order to assess the sensitivity of our results to sensor differences, we also compared results from the two altimeters. The procedure to extract water elevation from these altimeters is described next.

3.1.2.1. Jason-3 Water Level Extraction

The altimeter measures transit time of the transmitted microwave pulse after being reflected back from the water surface. The range, or distance between altimeter and water surface, is estimated from the round-trip travel time. While the on-board tracker continuously computes the midpoint of waveform's leading edge, the limited observation time and contamination from nonwater bodies inside radar footprint leads to a computational error. Hence, we employ a waveform retracking algorithm called ice retracking (Ice-1 retracker) to correct the estimated range from on-board tracker (Wang, 2019). The ice-retracked range is included in the distributed Jason-3 GDR data files. The ice-retracked range, R_{meas} , was then corrected for certain atmospheric and geophysical correction parameters, given by

$$R_{corr} = R_{meas} + \sum C_{Jason3} \quad (1)$$

$$\sum C_{Jason3} = C_{dry} + C_{wet} + C_{iono} + C_{pole} + C_{earth} \quad (2)$$

where R_{corr} is the corrected range, while C_{wet} , C_{dry} , and C_{iono} are the wet tropospheric, dry tropospheric and ionospheric corrections. C_{pole} and C_{earth} are polar tide and solid earth corrections, respectively. The corrected range is then converted to the water height h relative to the WGS 84 (World Geodetic Survey) referenced ellipsoid using the altimeter height H_{alt} . This is followed by a transformation from ellipsoidal to orthometric height using geoid height, H_{EGM} assuming reference as EGM 2008 (Earth Gravitational Model), given by

$$h = H_{alt} - R_{corr} - H_{EGM} \quad (3)$$

Minimum and maximum latitude bounds corresponding to the selected haors were specified along the altimeter pass to extract the height values across the haor. These height retrievals were averaged later to minimize the ensuing uncertainty.

3.1.2.2. Sentinel-3 Water Level Extraction

Extracting water levels from Sentinel-3 follows a similar procedure as explained for Jason-3 processing. The range correction is given as

$$\sum C_{Sentinel3} = C_{dry} + C_{wet} + C_{iono} + C_{earth} + C_{pole} \quad (4)$$

where the abbreviations are explained in section 3.1.2.1. To obtain the altimeter range using waveform retracking, we employ a robust retracking algorithm called Off Center of Gravity (OCOG). The OCOG retracked range is included in the enhanced measurement data file of Sentinel-3. As the Jason-3 water level extraction procedure has been established by Biswas et al. (2019), Sentinel-3 elevations were validated against those derived using Jason-3. The OCOG retracker in Sentinel-3 data corresponds to the Ice-1 retracker used in Jason-3 GDR (Crétau et al., 2018).

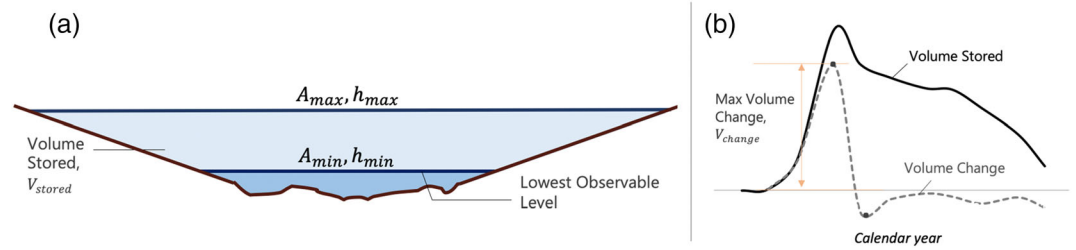


Figure 3. Illustration of (a) total volume stored relative to the lowest observable levels (light blue shaded area), and (b) maximum volume change over a calendar year for a typical haor.

The variables in the Jason-3 and Sentinel-3 data files that were used for the required corrections to extract water levels are summarized in Table S2 in the supporting information. The LOCSS/altimeter-based elevations and SAR-based area estimates were acquired to minimize the difference between their dates of acquisition. The mean difference in acquisition dates between the area and altimeter-derived elevation measurements was around 8.5 days. For haors where citizen scientists-derived (LOCSS) elevation was used, the difference was almost zero because of the near-daily frequency of LOCSS measurements.

3.1.3. Estimates of Volume Storage and Volume Change

Once the haor area and elevations are acquired on synchronous dates, variables that are hydrologically significant to the haor basin are estimated. These include (a) total volume of water storage across all the haors over a water year relative to their respective lowest observable levels, and (b) maximum seasonal volume change in the haors i.e. amount of water moving through the haor system in the water year. The haor volume is obtained by assuming a trapezoidal cross section owing to haors' relatively flat bathymetry in a terrain that is already very flat. The assumption of flat bathymetry is further corroborated by the depth-area relationship, which for a number of selected haors reveal flat-bottomed trapezoidal cross section (see Figure S2 of supporting information). To understand if this assumption regarding haor cross sections introduces nonnegligible uncertainty, we also derived and compared volume estimates assuming a rectangular cross section. Details of the comparison are provided in the supporting information (section S2).

The information on exact bottom topography of the haors was unavailable, which led us to estimate the volume storage with respect to the lowest observable level of the haors. Storage relative to the lowest level also addresses the differences in datum of elevation observed from altimeters and LOCSS gages. The lowest levels (h_{min}) of the haors were obtained over the period of record observed using altimeters or LOCSS (see Figure 3a). Thus, at a particular time, t , the volume stored, V_t , above the lowest level is given as

$$V_t = (h_t - h_{min}) * \frac{A_t + A_{min}}{2} \quad (5)$$

where h_t is the elevation obtained from Equation 3. Over a full water year, the maximum volume stored by a haor can thus be estimated as

$$V_{stored} = \max(V_t) \quad (6a)$$

$$V_{stored} = (h_{max} - h_{min}) * \frac{A_{max} + A_{min}}{2} \quad (6b)$$

where the maximum elevation (h_{max}) and maximum area (A_{max}) are obtained over all the days of a water year when the elevation and area observations were acquired. A similar volume estimation model was used by Baup et al. (2014) but assuming a triangular geometric shape for the lake's bathymetry. A triangular bathymetry was more appropriate the lake studied by Baup et al. because it was located in a region of much higher topographic relief.

The maximum volume change over a water year was then calculated as the maximum change in volume over consecutive acquisitions over the year. This signifies the amount of water that is moving through the haor system as surface water evaporation, groundwater recharge, exchange with connecting rivers, or

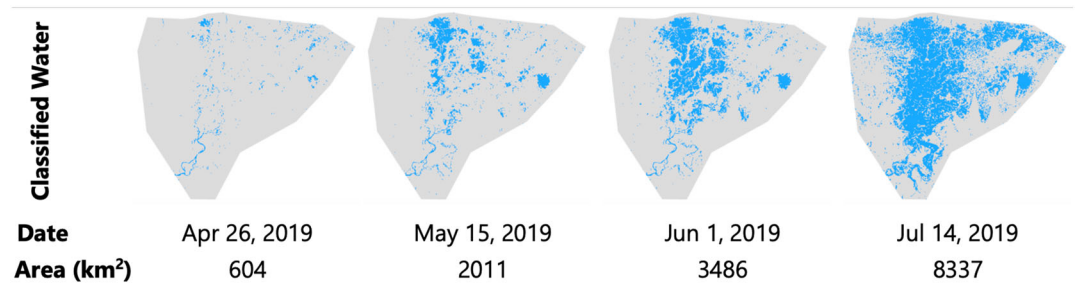


Figure 4. Evolution of open water (including haors) in the basin classified using Sentinel-1 SAR data during four different hydrological regimes and the respective area inundated by haors.

human use. The volume change is relevant when accumulated over all the haors, in particular for the overall groundwater recharge in the basin that controls the groundwater-based irrigation for rice cultivation. At any time step t , the change in volume stored from the previous acquisition date ($t - 1$) is given as

$$\Delta V_t = (h_t - h_{t-1}) * \frac{A_t + A_{t-1}}{2} \quad (7)$$

The maximum change in haor volume (V_{change}) was thus formulated as

$$V_{change} = \max(\Delta V_t) \quad (8)$$

where h_t is the haor level at time step t . An illustration of haor volume storage and change is provided in Figure 3.

3.2. Estimating Volume for All Haors in the Basin

Because the altimeter and LOCSS elevation data are limited in temporal and spatial extent, a regression-based approach was developed to map volumetric storage estimation across all the haors. The approach requires identifying haor boundaries to arrive at the probability distribution of their areas (section 3.2.2). This is followed by developing a statistical relationship between haor areas and their respective volumes estimated from section 3.1. Mapping this relationship over the areal distribution of all the haors provides statistically estimated total volume stored by the basin (section 3.2.3).

3.2.1. Water Delineation Using SAR Image

The first step toward estimating the cumulative storage in the entire haor basin is to classify the extent and count of all the haors. The procedure starts with delineating water bodies in the basin using SAR imagery over a season where most haors are in the early stage of development. As the season becomes wetter with the onset of monsoon rains and inundation expands, the adjacent haors merge to form large water bodies, making it difficult to classify the extent and boundaries of individual haors. Thus, the water delineation technique as described in section 3.1.1 was implemented over the entire haor basin for the premonsoon season (month of May 2019) when the haors just start to form. The year 2019 was a normal precipitation year, with annual precipitation comparable to the long-term climatology (Figure S5, supporting information). Sentinel-1 scenes mosaicked over the entire basin were used to classify the water area. It is worth mentioning here that although imagery for a single day was used to classify the haors, the algorithm was designed so as to account for the variations in haor extent over the year and generate an “average” extent of each haor in the basin. Figure 4 shows the evolution of open water in the basin, that also includes nonhaors such as rivers, classified using Sentinel-1 data during four different hydrological regimes.

3.2.2. Detection of Haor Extents—CoCoAH Technique

After obtaining the delineated open water in the basin using SAR imagery, the next stage is to identify the individual haor boundaries to use them for volumetric storage estimation. The remote sensing imagery used to classify the haors only provides a snapshot of the state of haors representative of the conditions at that moment. This poses a challenge in demarcating the haor extent with certainty as the inundation changes

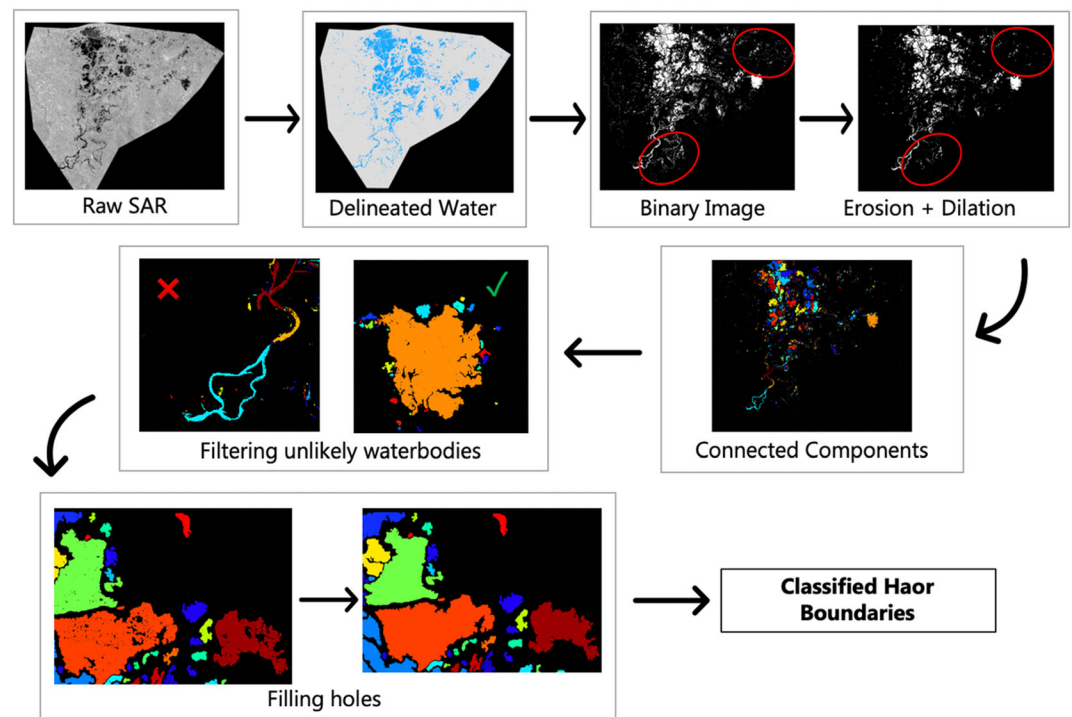


Figure 5. Overview of the steps involved in the Connected Components Analysis for Haors (CoCoAH) to classify haor boundaries.

during intraseasonal and interseasonal transition of hydrological regimes. To address the issue and generate robust haor extents, we implement here a novel algorithm based on the principles of digital image processing. This technique is termed as ‘Connected Components Analysis for Haors’ (CoCoAH). The individual steps involved in the proposed technique are shown in Figure 5 for sample SAR imagery over the haor basin.

3.2.2.1. Image Processing

CoCoAH first starts with converting the delineated water product into a binary image consisting of pixels that are labeled as logical ones (water) and zeros (nonwater). Next, to address the imperfect and dynamic nature of SAR-delineated water, morphological operators of erosion and dilation were applied to the binary image. The erosion operation erodes away the boundaries of water bodies to improve upon their edges and removes the noise caused by SAR speckle. Implementation of erosion requires specifying a binary valued neighborhood, called kernel. The value of the output pixel is the minimum value of all pixels in the kernel. A disk-shaped kernel with radius of 10 pixels, which corresponds to roughly 100 m, was selected. This radius is well suited for the study region because it is much smaller than the typical haor size, yet large enough to remove speckle noise. Next, the dilation operation fills up small holes (nonwater pixels) surrounded by a group of water pixels. The combined effect of the two operators, also termed as image opening, is to remove noises while retaining the shape and size of substantive features in the image.

The resulting image is then processed to find all the connected components that are potential candidates for being assigned as haors. MATLAB’s *bwconncomp* function was incorporated to find pixels that were connected with neighboring pixels. An eight-connected neighborhood was used which assigns adjoining pixels to same object.

3.2.2.2. Postprocessing

The connected component procedure results in a set of potential haors with varying shapes and sizes, but not all the connected objects can be labeled as haors. To arrive at the final set of haors, objects that are unlikely to be haors such as rivers, narrow channels, and smaller patches of water need to be discarded. This was achieved by performing a filtering operation based on three different properties of the connected component. These include circularity, eccentricity and object area. Circularity of a feature is defined as

Table 2
Threshold-Based Rules for Labeling Haors Imposed on the Properties of Area, Eccentricity, and Circularity of Connected Components

Property	Area (km ²)	Eccentricity	Circularity
Rule 1	Area ≥ 20	<0.925	no condition
Rule 2	0.2 < Area < 20	<0.95	>0.11

Note. Rules are mutually exclusive and either one getting satisfied for a water body labels it as a haor.

$$\text{Circularity} = \frac{\text{Perimeter}}{2\sqrt{\pi \cdot \text{Area}}} \quad (9)$$

while the eccentricity is given by

$$\text{Eccentricity} = \frac{\text{distance between foci}}{\text{major axis length}} \quad (10)$$

Rivers and other narrow channels exhibit low circularity and high eccentricity, while for haors, the circularity is generally high with low eccentricity. Also, objects with very small area are potential noise/temporary water, unlikely to be haors. Typical values of these properties for haors and rivers are shown in Figure S3 in the supporting information. Based on this observation, thresholds were selected for each property to label the objects as haors versus non-haors. These threshold-based rules are tabulated in Table 2. As a final step, image filling was performed to remove any remaining holes (missed by the water delineation algorithm over the SAR imagery) within the objects labeled as haors to produce a robust extent for each haor. Based on the classified haor boundaries, a probability distribution function (PDF) was derived for areal extent of all the haors.

3.2.3. Volume-Area Relationship

Because it is not feasible to obtain elevation estimates for all the haors in the region with currently available remote sensing products, volume estimations for haors selected in section 3.1 were used to derive a statistical

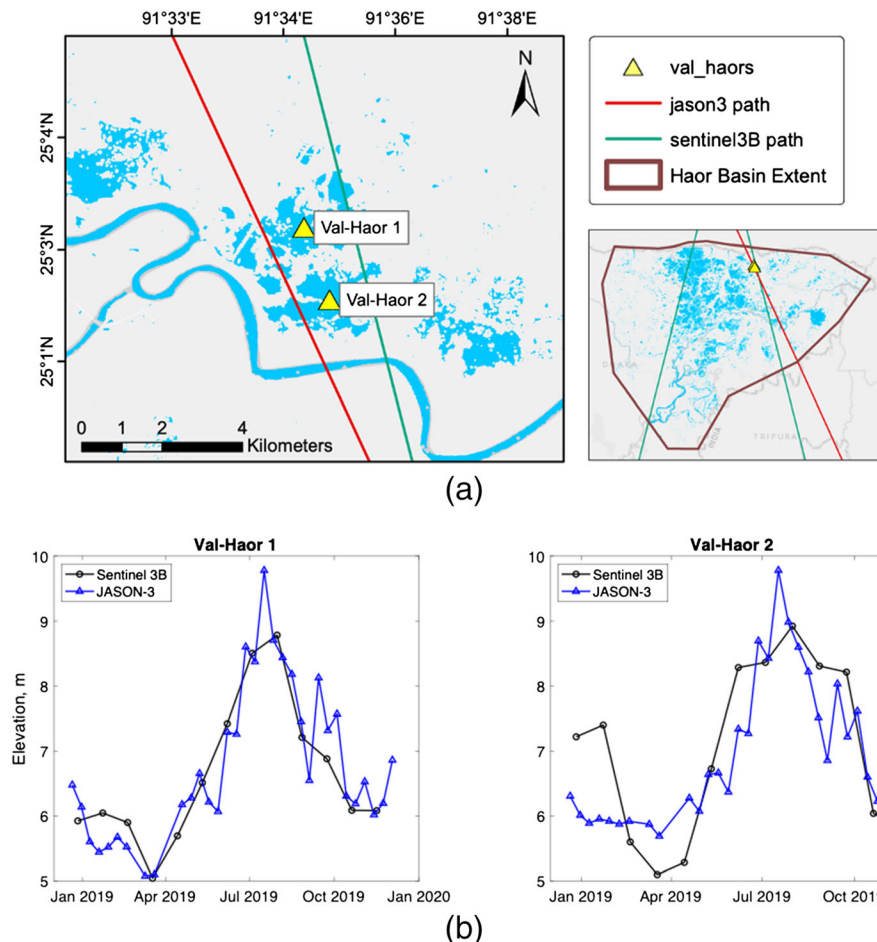


Figure 6. (a) Haors selected for validating (comparing) elevation extraction procedure from Sentinel-3B against Jason-3. (b) Validation of Sentinel-3 water level retrievals against Jason-3 for the two haors used for validation.

Table 3
Metrics for Comparison of Sentinel-3 and Jason-3 Water Level Retrievals for Two Haors

Metric	Val-Haor 1	Val-Haor 2
RMSE (m)	0.47	0.67
Mean absolute error (MAE) (m)	0.34	0.55
Pearson's correlation	0.92	0.86

volume versus area relationship (see Figure 11). To account for the inter-annual variability and uncertainty in hydrological response of the haors, we used volumetric estimates for each available year to develop this relationship. We obtained uncertainty estimates in the regression coefficient of the least squares fit to derive the area-volume relationship with 95% confidence interval. The uncertainty in regression coefficient allows to consider the dispersion of scatter plot while fitting the regression relationship, although, it does not explicitly model the biases or errors in acquired

sample points of volume or area. Details of deriving the uncertainty estimates are provided in the supporting information (section S1). This relation was then used to extrapolate volumes for all the remaining haors in the region using their respective areas obtained from the CoCoAH technique.

3.3. Assessment of Volume Estimates

The accuracy of the overall estimated haor volume was assessed using high-resolution (3 m) PlanetScope imagery, combined with the satellite altimetry data already described in section 3.1.2. No accuracy assessment of elevation data in individual haors was possible due to a lack of in situ measurements in the region or other sources of validation data. The Planet imagery has its own limitation as a reference, such as the product's optical nature, which can lead to biases in the derived water volume (Houborg & McCabe, 2018). Nevertheless, the high spatial resolution imagery is the best option available to assess the accuracy of volume variations associated with different methods of haor classification and inundation extent calculation. PlanetScope scenes with four bands in the visible and Near Infrared (NIR) wavelengths were downloaded over a portion of haor basin for two different days representing evolving stages of haors (growing to fully mature) in the basin (see Figure 4). To minimize biases, we acquired cloud-free scenes on days synchronous with the respective acquisition dates of area and elevation measurements.

To delineate water in the acquired Planet scenes, we performed supervised classification on each image using maximum likelihood classification technique, similar to that used in our previous study (Ahmad et al., 2019). Training was performed by manually labeling a set of pixels as water and nonwater. The CoCoAH technique was then applied over the classified reference Planet imagery to delineate the haor boundaries and obtain the statistical distribution of their respective areas. Finally, using the volume-area relationship developed earlier, the total volume across all haors was obtained and compared with that from the SAR-based volume estimates over the same region. Additionally, spatial maps were visually compared to evaluate spatial consistency of classification.

Another source of validation for the remote sensing-based estimates were the haors identified from the official master plan of the haor basin in northeastern Bangladesh (Master Plan of Haor Area Volume II, Summary Report, 2012). This institutional master plan identifies a total of 373 haors in the northeast region and tabulates their respective areas. It does not, however, include volume estimates. We derived haor volumes from the stated areas of haors in the plan using the developed area-volume relationships from section 3.2.3. Because the haors included in the master plan represent the mature stage of development, we compared the overall volumetric storage estimate against results from remote sensing (SAR) imagery for the wettest of the 3 days selected in the present study (14 July 2019).

4. Results

4.1. Haor Volume Using LOCSS and Remote Sensing

The area obtained from backscatter-based thresholding on Sentinel-1 imagery for the 13 selected haors were used in conjunction with the elevation retrievals from LOCSS and altimetry to estimate haor volume. Results for respective elevation, area, and volume estimates are described in the following sections.

4.1.1. Assessment of Sentinel-3 Elevation Extraction

The procedure for extracting water levels from Sentinel-3 data was compared against the retrievals from Jason-3 for haors crossed by both the altimeter tracks. Two such haors are shown in Figure 6a. One of these haors varies in areal extent from 1.3 to 9.5 km² and the other from 0.6 to 6.1 km² over the course of dry and wet seasons. The heights from Jason-3 were validated by Biswas et al. (2019) over 12 virtual stations in Southeast Asia out of which one of the stations, Annapurnaghat on the Barak River of India, is located on

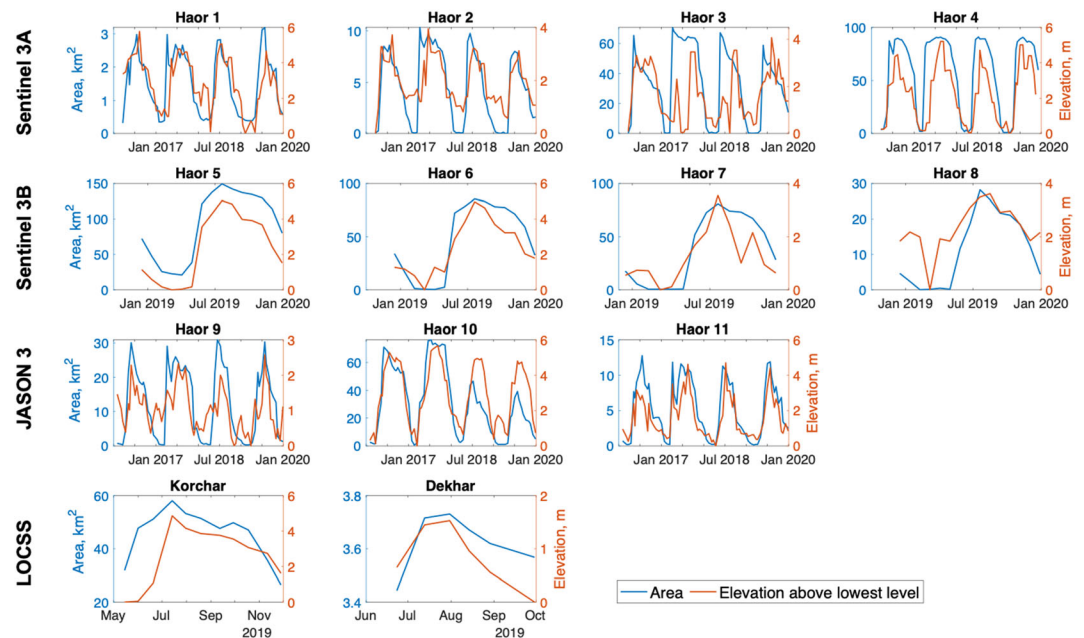


Figure 7. Area (km^2 ; left axis) and elevation above lowest observable level of haors (m; right axis) extracted using remote sensing or LOCSS data for selected haors (see Figure 1 and Table 1 for locations).

a river system directly connected to the haors. The comparison allows us to assess the sensitivity of elevation measurements to differences in sensor characteristics. Because Sentinel-3B passes in close proximity to Jason-3, the assessment was performed for the year 2019, when Sentinel-3B data were available.

The water levels extracted from the two sources are shown in Figure 6b for both the haors. The metrics of root-mean-square error (RMSE), mean absolute error (MAE), and Pearson's correlation used for comparison are summarized in Table 3.

4.1.2. Area and Elevation Extraction

The time series for area from Sentinel-1 SAR imagery and elevation from LOCSS/Jason-3/Sentinel-3A/Sentinel-3B altimeters for selected haors are shown in Figure 7. The elevations in Figure 7 are shown relative to the lowest observable levels of the respective haors. The Sentinel-3B and LOCSS elevations are available over the year 2019 while Jason-3 and Sentinel-3A were acquired over 2016–2019.

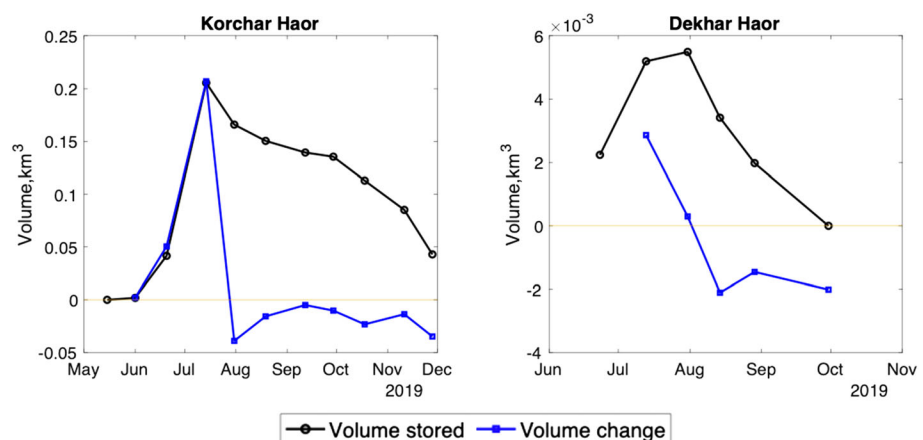


Figure 8. Volume stored (in black) and volume change (in blue) derived using SAR-based area and citizen science elevation data for 2019 for two haors monitored under LOCSS project.

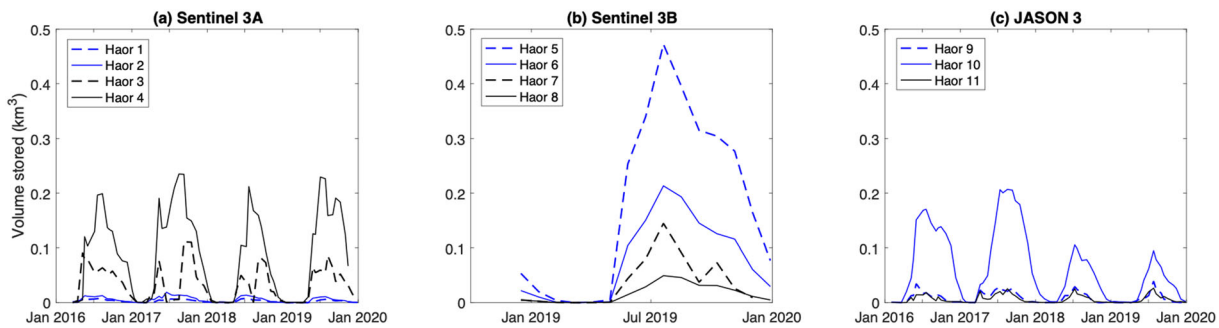


Figure 9. Volumetric storage derived using SAR-based area and altimeter-based elevation for haors relative to lowest observable levels selected along the altimeter passes of (a) Sentinel-3A, (b) Sentinel-3B, and (c) Jason-3 (see Figure 1 and Table 1 for the location of haors passed by each sensor).

4.1.3. Volumetric Storage Estimation

Using the area and elevation estimates, the total volume stored and maximum volume change in each haor over each water year was derived using Equations 5–8. The time series of the volume stored and volume change over the water year of 2019 for haors of LOCSS project are shown in Figure 8.

As mentioned earlier, the volume change signifies the total flux of water from haors through surface water evaporation, groundwater recharge, exchange with river, and human use, while gain in storage occurs with rainfall events over the monsoon season. For the other haors along the altimeter passes (refer to Figure 1 for pass locations), the volume storage estimates are shown in Figure 9. We do not show the respective volume changes for these haors for the sake of brevity. Interannual variations in the haor volume storage and volume changes over the available period of observations (2016–2019 for Sentinel-3A/Jason-3, 2019 for Sentinel-3B/LOCSS) are shown in Figure S4 in the supporting information.

The large differences in volumetric storage across the selected haors suggest that, aside from the dominant seasonal signal apparent in all haors, the basin contains haors with varying hydrological signatures. These differences reflect variations in hydrologic processes driving haor storage and also govern the basin's variable groundwater recharge and livelihood patterns.

4.2. Volume Estimation for Entire Haor Basin

Based on the limited set of haors available for volumetric storage estimation via altimetry, SAR imagery, and citizen science data, the next step is to scale up the estimates to the entire haor basin. This starts with the detection of haor boundaries in the basin using CoCoAH to obtain their areal extents (section 4.2.1) and then develop an empirical relationship between area and volume based on the volume estimates over haors from section 4.1 (see section 4.2.2). Using the relationship, the volumetric storage was derived for all the haors in the basin (section 4.2.3).

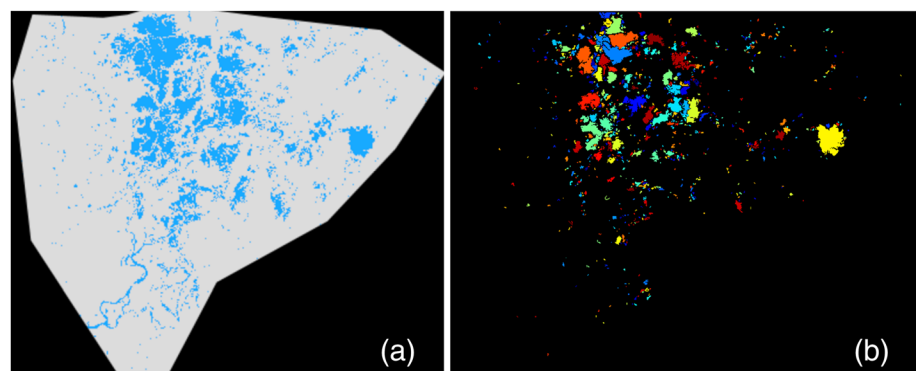


Figure 10. Resulting classified haors (right panel; b) using the CoCoAH technique based on delineated water from Sentinel-1 SAR imagery (left panel; a). The colors are randomly assigned to the classified haors.

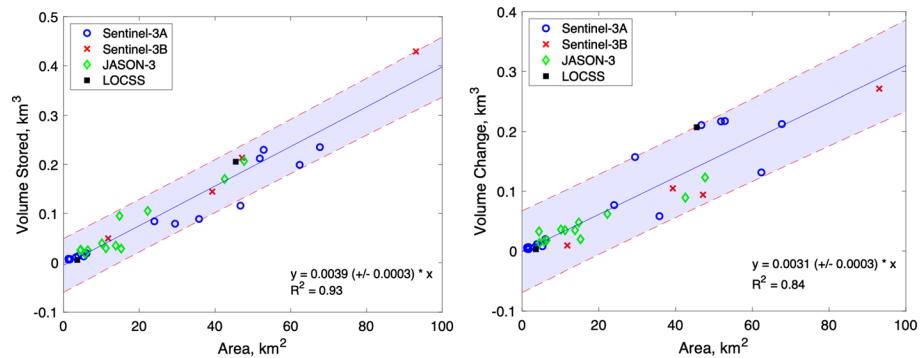


Figure 11. Relationship of haor area with the respective volume storage (left panel) and volume change (right panel) shown for haors with different sources of elevation measurements. Area between red dashed lines represent 95% confidence bounds for regression coefficients.

4.2.1. CoCoAH for Haor Detection

The baseline for the CoCoAH technique was established by implementing it over the haor basin on 22 May 2019 when the haors were still in the growing stage. Following the stepwise procedure described in section 3.1.2, the resulting classified haors are shown in Figure 10.

The results obtained on haor extent detection were used to derive the statistical distribution of areas for all the detected haors. A total of 760 haors were detected by the CoCoAH technique for the selected date when the haors were in the formative stages at the onset of the monsoon season.

4.2.2. Volume-Area Relationship

Based on the volume estimates for individual haors from section 4.1 for each available water year, a total of 34 points for area and volume storage/change were plotted to reveal a strong linear relationship. The intercept for the empirical relationship was set to zero to ensure physically feasible volume estimates for haors with smaller areas. To include uncertainty estimates, 95% confidence intervals have also been plotted for coefficient (slope) of the least squares fit (also see supporting information section S1). Figure 11 shows this relationship of area with haor volume storage and change.

The area and volumetric storage exhibit strong linear dependence, with a correlation of 0.93. This relationship underlines the relatively flat bathymetry of the haors in the basin that causes the volume to increase linearly with the spatial extent of haor. The volume change across the season follows a similar linear relationship with the area of haors but with higher uncertainty. Haors for which water surface height was measured using citizen science and using satellite altimetry fall along the same best fit lines in Figure 11, suggesting that both methods provide consistent data for estimating haor volume.

4.2.3. Volumetric Estimates for All Haors and Their Seasonal Variability

Using this relationship and delineated haor extents from CoCoAH technique, we estimated volume for all the detected haors. The analysis resulted in a cumulative volume of $6.5 \pm 0.4 \text{ km}^3$ across the 760 detected

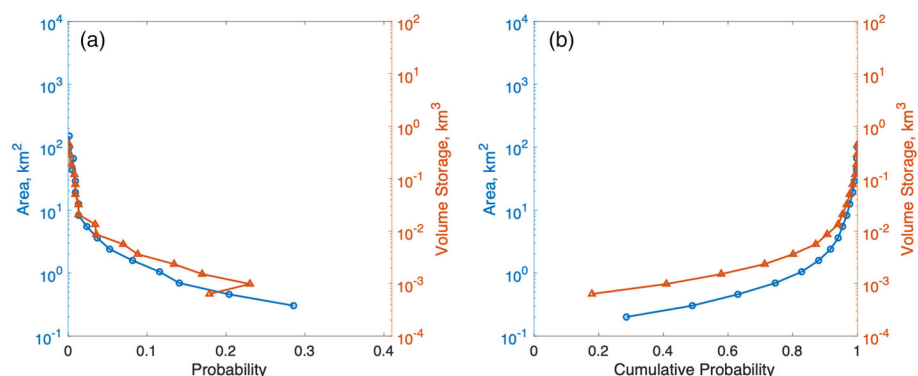


Figure 12. (a) PDF and (b) CDF of area and total volume storage over the classified 760 haors in the basin for 22 May 2019.

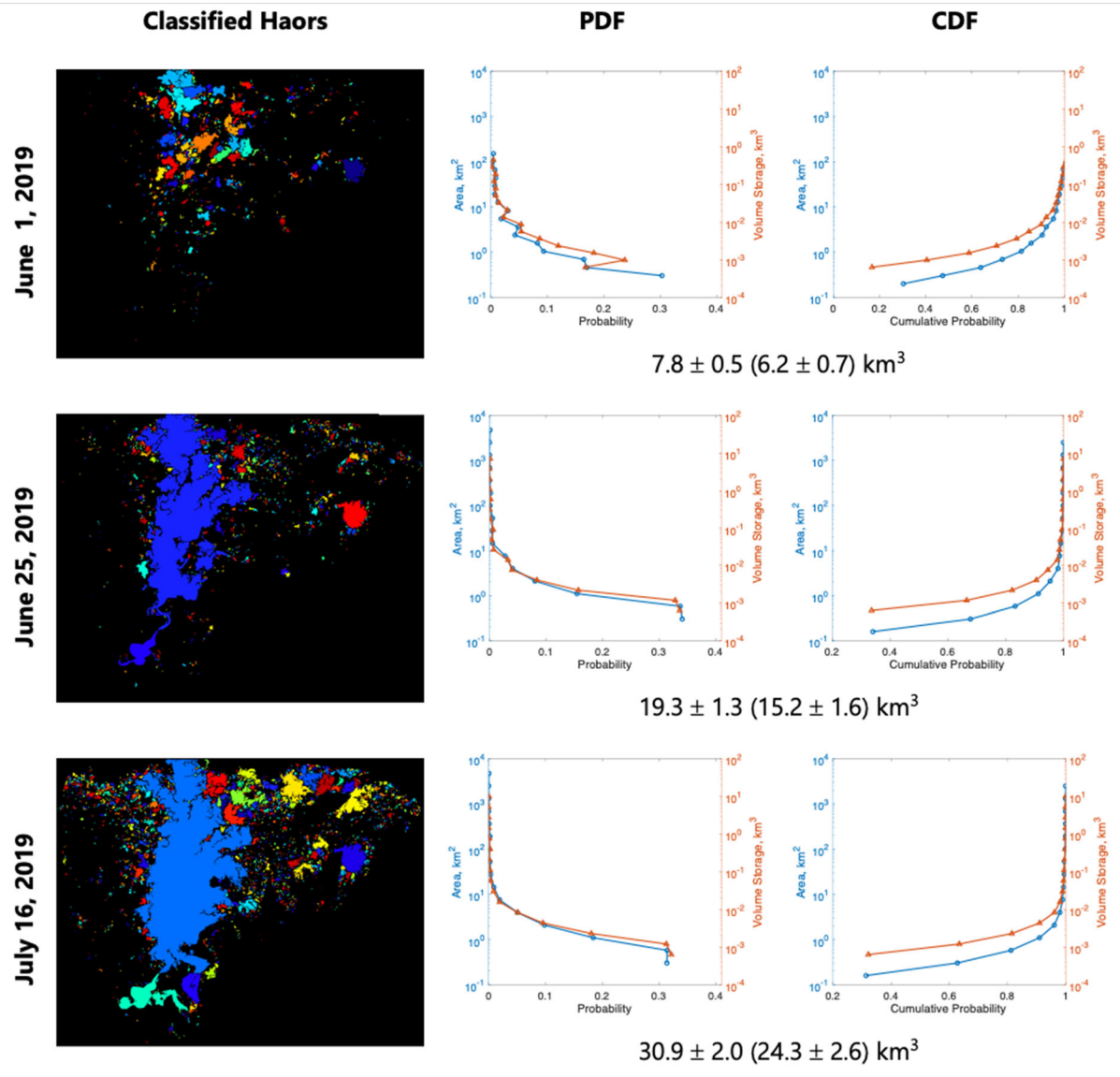


Figure 13. Classified haors (left panels), PDF (middle panels), and CDF (right panels) of area and volume storage over different days representing evolving stages of haor. Cumulative volume storage relative to the lowest observable level (with volume change in brackets) is shown below the distribution plots. Colors are randomly assigned to the classified haors.

haors during the onset of the wet season. The corresponding cumulative volume change was $5.1 \pm 0.5 \text{ km}^3$. The statistical probability and cumulative distribution functions (PDF and CDF, respectively) of the haor area and resulting volume storage over the haors is shown in Figure 12.

To capture the intraseasonal variability of volumetric estimates for haors during the monsoon season, the analysis was repeated for three other days. These days were representative of the different stages (early, growing, or mature) of haor's annual lifecycle. The resulting haor extents for different stages and the statistical distribution of area and volume storage are shown in Figure 13. Cumulative haor volume storage is also shown for all the classified haors in the basin.

The cumulative volume relative to the lowest observable level increases to $30.9 \pm 2.0 \text{ km}^3$ (corresponding to the mature stage in July considered here) as the haors develop over the course of water year. To put the figures in perspective, such a volumetric storage exceeds the volume of all but 10 lakes in the United States and is equal to the active storage held behind the Three Gorges Dam or three Grand Coulee Dams. As the season

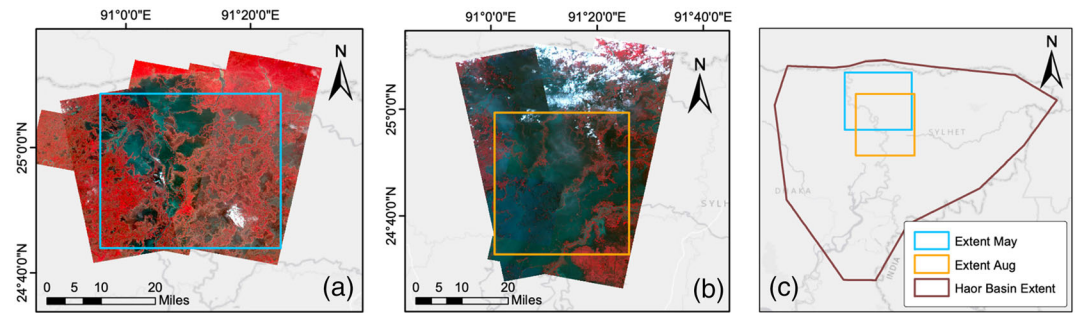


Figure 14. False Color Composite of mosaicked Planet images acquired on (a) 15 May 2019 (early stage) and (b) 26 August 2019 (developed stage) over footprints as shown in (c) over haor basin.

becomes wetter, the adjacent haors merge to form a large water body, flooding a major portion of the basin. This also leads to an increase in the cumulative volume storage in the basin by almost 5 times when the haors are in their mature stage.

4.3. Comparison Against Higher Resolution Data

The sensitivity of estimated haor volumes to area estimates from Sentinel-1 was assessed using areas calculated from PlanetScope imagery. Planet images were acquired for two different days - one during the early stage in May 2019 and another after the haors fully develop in August 2019. Due to computational limitations in acquiring Planet scenes over the entire Haor basin, a smaller subset of the basin was selected for the analysis where potential cloud-free scenes were available. The mosaicked products are shown in Figure 14.

The CoCoAH analysis was performed on the Planet images after delineating water using supervised classification. The resulting haor extents were used as reference to assess the volume estimation based on SAR imagery over the closest synchronous days. The comparison of classified haor extents, estimated volume storage and volume change on the 2 days are shown in Figure 15. Table 3 summarizes the absolute and percentage errors in Sentinel-1 based haor extents when compared with extents from Planet imagery.

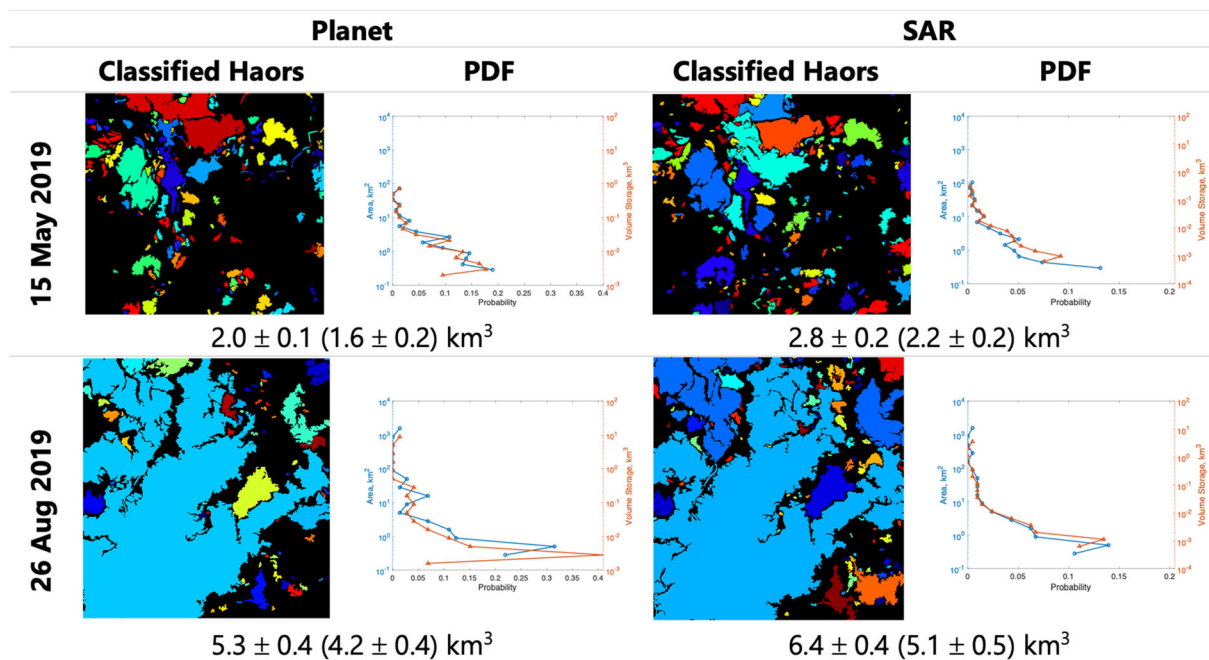


Figure 15. Comparison of haor classification based on SAR (Sentinel-1) and Planet imagery over two different days in terms of haor extents and PDF of haor area and volume storage. Cumulative volume storage is shown below the histograms with respective volume change in parentheses. Colors are randomly assigned to the classified haors.

Table 4
Quantitative Assessment of Haor Classification Based on Sentinel-1 Imageries

Date of acquisition	Reference	Absolute error (km ³)	Percentage error
15 May 2019	Planet	0.8	40.0%
26 August 2019	Planet	1.1	20.7%
16 July 2019	Master Plan	2.2	6.7%

Note. Errors (absolute and percentage) are calculated using haor volumes derived from Planet imagery and Master plan from government records as reference.

Although both the SAR and high-resolution Planet-derived volume estimates have inherent limitations, the resulting volume estimates from the two sources were found to be comparable. The SAR estimates are somewhat higher than the Planet estimates, which might be explained by the larger impact of vegetation on Planet imagery than on Sentinel-1 imagery. The statistical distribution (PDF) of haor areas and volumes also matches closely. The errors reduce as the haors evolve into the wetter season. It should be noted here that the assessment is dependent on the accuracy of supervised classification performed over the Planet imagery, as established by Ahmad et al. (2019).

Finally, we compared the volumetric estimates against the available government records in the master plan for the haor basin. Using the area-volume relationships derived in Figure 11, the total volume stored in the basin from master plan was found to be $33.0 \pm 1.7 \text{ km}^3$, while that from the SAR-based haor classification (for the wettest day) was $30.8 \pm 1.6 \text{ km}^3$. This signifies that the SAR-based inundation closely approximates the figures reported in the master plan over the wet seasons when most of the haors are fully evolved. The difference between the two methods is small despite the fact that the measurements of haor area were acquired over different time periods. However, the large number of haors classified from SAR imagery in comparison to the master plan are due to a higher frequency of haors with low volumes produced by our technique (see Figure 13 for the distribution of remotely sensed haor volumes). The errors between SAR-based inundated extent and that recorded in the Master Plan are also summarized in Table 4.

5. Discussion and Conclusions

This study presented a cost-effective approach using citizen science and satellite remote sensing data to estimate the volume of water stored in seasonal wetlands impacted by transboundary runoff. Total volumetric storage and change in these seasonal wetlands or haors carry fundamental hydrological significance for developing physical understanding of wetland processes and also controls livelihoods and ecosystems in the region. The set of haors under the combined sampling of citizens and satellites revealed a consistently strong linear dependence between the haor's areal extent and its volumetric storage. Over the selected analysis days in water year 2019, the total haor volume storage, relative to the lowest observable level, ranged from $6.5 (\pm 0.4)$ to $30.9 (\pm 2.0) \text{ km}^3$ as the haors formed and expanded during the monsoon season. To put this in perspective, the volumetric storage during the wettest season is comparable to the active storage held behind the Three Gorges Dams in China or three Grand Coulee Dams in the United States.

The empirical relationship derived here to scale up the volume estimates over a larger number of haors based on citizen science, satellite data, and automated classification provides a practical approach for implementing the same over numerous other small and large wetlands around the globe. Our study indicates that the potential of synergistically using citizen science and remote sensing data is encouraging, as demonstrated here over northeastern Bangladesh, because it is able to reveal a previously unknown insight on volumetric storage with a high degree of confidence. We should stress that there has been no reported study, to the best of our knowledge, performed on such a large number of highly dynamic floodplain lakes or wetlands to determine their volumetric storage and temporal variation over multiple years.

The findings presented here have implications for ecosystem-sensitive and livelihood-centric water management policies in the region. Given the existing gaps in terms of utilizing the abundant natural resources (Master Plan of Haor Area Volume I, 2012), information on the amount of water storage over the water year can help inform better policies of water use for rice and fish production while maintaining ecosystem services. One of the potential direct consequences of our ability to report on volumetric storage and change is improvement in irrigation practices that usually take place during the dry season using groundwater recharged from the preceding monsoon season. During the wet season, the total storage provides an idea of the amount of groundwater recharge and can help determine the available supply of sustainable groundwater for irrigation during dry season. The survival and breeding of aquatic species also depend heavily on the amount of water stored by these haors (Thilsted & Wahab, 2014). Incorporating volume estimates in

water resource management policies can not only result in smarter water use practices for humans but also improve ecosystem services.

The accuracy of the volumetric estimates depends upon the confidence in remote sensing based areal extents, performance of image processing in delineating the haors, and elevation measurements from radar altimeters and citizen scientists. The choice of haor cross section is critical for the volumetric estimates and can introduce significant uncertainty. Our investigation on the impact of bathymetry revealed that a rectangular cross section can result in up to 47% higher volumetric storage compared to a trapezoidal (refer to section S2 and Table S1 in the supporting information). Hence, it is critical for studies on such flat-bottomed seasonal haors to err on the side of caution and assume a trapezoidal cross section (which is corroborated by the depth-area relationships shown in Figure S2) for conservative volumetric estimates.

The side-looking geometry and the requirement for specular reflection can result in misclassification of water due to the presence of vegetation (e.g., hyacinth) on water or due to its uneven surface. Another source of uncertainty is the choice of rules and thresholds imposed upon the properties of connected components to filter haors from water bodies unlikely to be haors. The altimeter elevation extraction procedure introduces biases from the errors in the geoid height model as well as imperfect geophysical and atmospheric corrections. Other sources of uncertainty include errors due to different time samplings between the satellite missions used, the linear relationship between area and volume for the observed haors and the assumption that this relationship could be used for all unobserved haors.

While there are no previous studies to specifically derive the volume estimate of wetlands in Bangladesh, we compared our results with those found by Baup et al. (2014) over a single lake with mean extent of 0.52 km^2 in southwest France. The study derived an empirical second-degree polynomial relationship between volume and lake area with a correlation of 0.90, in comparison to the correlation of 0.93 obtained in our study using linear fit over multiple haors. While the study of Baup et al. (2014) has key differences in terms of altimeter mission used (Envisat) and lake size ($<1 \text{ km}^2$), the comparison is still valuable in underscoring the need to develop improved relationships between lake volume and area. Further, comparing the lake volume variations, Crétau et al. (2016) reported a cumulative volume storage of around 40 km^3 over 11 lakes in Tibetan Plateau during a period of 20 years. Comparing this to a similar volume change of haor basin but at a seasonal scale in our study signifies the highly dynamic behavior of these haors in the tropical monsoon climate.

The concept presented on synergistic use of elevations from citizen science and remote sensing with satellite-based area measurements will be of particular interest in the near future with the launch of new satellite missions. The most relevant of the future missions is the Surface Water and Ocean Topography (SWOT) mission scheduled to launch in 2022. The SWOT mission is expected to provide simultaneous water surface elevation and inundation extent data over nearly the entire global land surface (Biancamaria et al., 2016). Because SWOT is a wide-swath altimeter, it will provide an unprecedented data set on variations in lake area, height, and volume that can be used with the proposed approach to estimate volume storage and change at high temporal frequency for numerous small and large lakes/wetlands. While this study observed storage variations in 13 haors and inferred variations in hundreds of others, SWOT will directly observe variations in all but the smallest haors studied here. Another satellite mission planned for launched is NASA-ISRO (Indian Space Research Organization) Synthetic Aperture Radar (NISAR) (Rosen et al., 2016, 2017). The mission includes an L-band imagery that promises to precisely measure changes in surface water heights under vegetation (Alsdorf et al., 2000, 2005) and groundwater storage as well as to map the lake extents. A combination of SWOT and NISAR has the potential to allow accurate space-based monitoring of water resources for monsoonal environments of South Asia as well as for global scale applications.

Data Availability Statement

Citizen science data are available online (at www.locss.org). All other data used in this study are publicly available. Satellite remote sensing data from Jason-3 altimeter platform are available from Physical Oceanography DAAC (PO.DAAC) online (at https://podaac.jpl.nasa.gov/dataset/JASON_3_L2_OST_OGDR_GPS). Sentinel-3 altimeter data are available online (from <https://sentinel.esa.int/web/sentinel/sentinel-data-access>). Landsat data were acquired from Google Earth Engine repository. Planetscope optical data were downloaded from planet.com after making a request.

Acknowledgments

This work was supported by NASA Citizen Science for Earth Systems Program grant 80NSSC18M0099 “Tracking Freshwater Storage in Lakes: Citizens and Satellites Implementation Phase.”

References

- Ahmad, S. K., Hossain, F., Eldardiry, H., & Pavelsky, T. M. (2019). A fusion approach for water area classification using visible, near infrared and synthetic aperture radar for South Asian conditions. *IEEE Transactions on Geoscience and Remote Sensing*, 58(4), 2471–2480.
- Alsdorf, D. E., Dunne, T., Melack, J. M., Smith, L., & Hess, L. (2005). Diffusion modeling of recession flow on central Amazonian floodplains. *Geophysical Research Letters*, 32, L21405. <https://doi.org/10.1029/2005GL024412>
- Alsdorf, D. E., Melack, J. M., Dunne, T., Mertes, L. A., Hess, L. L., & Smith, L. C. (2000). Interferometric radar measurements of water level changes on the Amazon flood plain. *Nature*, 404(6774), 174–177. <https://doi.org/10.1038/35004560>
- Amezaga, J. M., Santamaria, L., & Green, A. J. (2002). Biotic wetland connectivity—Supporting a new approach for wetland policy. *Acta Oecologica*, 23(3), 213–222.
- Baup, F., Frappart, F., & Maubant, J. (2014). Combining high-resolution satellite images and altimetry to estimate the volume of small lakes. *Hydrology and Earth System Sciences*, 18(5), 2007.
- Bennett, S., Scott, D., Karim, A., Sobhan, I., Khan, A. & Rashid, S. M. A. (1995). Wetland resources specialist study, northeast regional water management plan. Bangladesh Flood Action Plan (FAP)-6, Bangladesh.
- Biancamaria, S., Lettenmaier, D. P., & Pavelsky, T. M. (2016). The SWOT mission and its capabilities for land hydrology. In *Remote sensing and water resources* (pp. 117–147). Cham: Springer.
- Birkett, C. M., & Beckley, B. (2010). Investigating the performance of the Jason-2/OSTM radar altimeter over lakes and reservoirs. *Marine Geodesy*, 33(S1), 204–238.
- Biswas, N. K., Hossain, F., Bonnema, M., Okeowo, M. A., & Lee, H. (2019). An altimeter height extraction technique for dynamically changing rivers of South and South-East Asia. *Remote Sensing of Environment*, 221, 24–37.
- Brakenridge, R., & Anderson, E. (2006). MODIS-based flood detection, mapping and measurement: The potential for operational hydrological applications. In *Transboundary floods: Reducing risks through flood management* (pp. 1–12). Dordrecht: Springer.
- Brown, O. B., & Cheney, R. E. (1983). Advances in satellite oceanography. *Reviews of Geophysics*, 21(5), 1216–1230.
- Bullock, A., & Acreman, M. (2003). The role of wetlands in the hydrological cycle. *Hydrology and Earth System Sciences*, 7(3), 358–389. <https://doi.org/10.5194/hess-7-358-2003>
- Chen, Y., Huang, C., Ticehurst, C., Merrin, L., & Thew, P. (2013). An evaluation of MODIS daily and 8-day composite products for floodplain and wetland inundation mapping. *Wetlands*, 33(5), 823–835.
- Chen, L., Jin, Z., Michishita, R., Cai, J., Yue, T., Chen, B., & Xu, B. (2014). Dynamic monitoring of wetland cover changes using time-series remote sensing imagery. *Ecological Informatics*, 24, 17–26. <https://doi.org/10.1016/j.ecoinf.2014.06.007>
- Chipman, J. W. (2019). A multisensor approach to satellite monitoring of trends in lake area, water level, and volume. *Remote Sensing*, 11(2), 158.
- Crétau, J. F., Abarca-del-Río, R., Berge-Nguyen, M., Arsen, A., Drolon, V., Clos, G., & Maisongrande, P. (2016). Lake volume monitoring from space. *Surveys in Geophysics*, 37(2), 269–305.
- Crétau, J. F., Berge-Nguyen, M., Calmant, S., Jamangulova, N., Satylkanov, R., Lyard, F., et al. (2018). Absolute calibration or validation of the altimeters on the Sentinel-3A and the Jason-3 over Lake Issykkul (Kyrgyzstan). *Remote Sensing*, 10(11), 1679.
- Dewan, A. M., Islam, M. M., Kumamoto, T., & Nishigaki, M. (2007). Evaluating flood hazard for land-use planning in Greater Dhaka of Bangladesh using remote sensing and GIS techniques. *Water Resources Management*, 21(9), 1601–1612.
- Du, Y., Zhang, Y., Ling, F., Wang, Q., Li, W., & Li, X. (2016). Water bodies' mapping from Sentinel-2 imagery with modified normalized difference water index at 10-m spatial resolution produced by sharpening the SWIR band. *Remote Sensing*, 8(4), 354.
- Dwarakish, G. S., & Ganasri, B. P. (2015). Impact of land use change on hydrological systems: A review of current modeling approaches. *Cogent Geoscience*, 1(1), p.1115691.
- Fienen, M. N., & Lowry, C. S. (2012). Social.Water—A crowdsourcing tool for environmental data acquisition. *Computers & Geosciences*, 49, 164–169. <https://doi.org/10.1016/j.cageo.2012.06.015>
- Gao, H., Wang, L., Jing, L., & Xu, J. (2016). An effective modified water extraction method for Landsat-8 OLI imagery of mountainous plateau regions. *IOP Conference Series: Earth and Environmental Science*, 34, 012010. <https://doi.org/10.1088/1755-1315/34/1/012010>
- Gaupp, F., Hall, J., & Dadson, S. (2015). The role of storage capacity in coping with intra-and inter-annual water variability in large river basins. *Environmental Research Letters*, 10(12), p.125001.
- Gorelick, N., Hancher, M., Dixon, M., Ilyushchenko, S., Thau, D., & Moore, R. (2017). Google Earth Engine: Planetary-scale geospatial analysis for everyone. *Remote Sensing of Environment*, 202, 18–27.
- Hossain, A. K. M. A. (2013). Flood inundation and crop damage mapping: A method for modeling the impact on rural income and migration in humid deltas. In F. Hossain, & R. Pielke Sr. (Eds.), *Climate vulnerability: Understanding and addressing threats to essential resources* (Chap 5.36, 1st ed., pp. 357–374). New York: Elsevier Inc., Academic Press.
- Houborg, R., & McCabe, M. F. (2018). A cubesat enabled spatio-temporal enhancement method (CESTEM) utilizing planet, landsat and modis data. *Remote Sensing of Environment*, 209, 211–226.
- Huang, C., Chen, Y., Wu, J., Li, L., & Liu, R. (2015). An evaluation of Suomi NPP-VIIRS data for surface water detection. *Remote sensing letters*, 6(2), 155–164.
- Huang, C., Chen, Y., Zhang, S., & Wu, J. (2018). Detecting, extracting, and monitoring surface water from space using optical sensors: A review. *Reviews of Geophysics*, 56, 333–360. <https://doi.org/10.1029/2018RG000598>
- Kamal, A. M., Shamsudduha, M., Ahmed, B., Hassan, S. K., Islam, M. S., Kelman, I., & Fordham, M. (2018). Resilience to flash floods in wetland communities of northeastern Bangladesh. *International Journal of Disaster Risk Reduction*, 31, 478–488.
- Kamruzzaman, M., & Shaw, R. (2018). Flood and sustainable agriculture in the Haor basin of Bangladesh: A review paper. *Universal Journal of Agricultural Research*, 6(1), 40–49.
- Kaplan, G. & Avdan, U. (2018). Sentinel-1 and Sentinel-2 data fusion for wetlands mapping: Balıkdami, Turkey. International Society for Photogrammetry and Remote Sensing (ISPRS) TC III Mid-term Symposium “Developments, Technologies and Applications in Remote Sensing”, 7–10 May, Beijing, China.
- KlogoGriffith, S., Akpeko, G., & Isaac, A. K. E. (2013). On the performance of filters for reduction of speckle noise in SAR images of the coast of the Gulf of Guinea. *International Journal of Information Technology, Modeling and Computing*, 1(4), 43–52.
- Liu, C. (2016). *Analysis of Sentinel-1 SAR data for mapping standing water in the Twente region*. Enschede, The Netherlands: University of Twente.
- Lowry, C. S., & Fienen, M. N. (2013). CrowdHydrology: Crowdsourcing Hydrologic Data and Engaging Citizen Scientists. *Ground Water*, 51(1), 151–156. <https://doi.org/10.1111/j.1745-6584.2012.00956.x>

- Lowry, C. S., Fienen, M. N., Hall, D. M., & Stepenuck, K. F. (2019). Growing pains of crowdsourced stream stage monitoring using mobile phones: The development of CrowdHydrology. *Frontiers in Earth Science*, 7, 128.
- Master Plan of Haor Area Volume I, Summary Report (2012). *Center for environmental and geographic information services*. Bangladesh: Bangladesh Haor and Wetland Development Board.
- Master Plan of Haor Area Volume II, Summary Report (2012). *Center for environmental and geographic information services*. Bangladesh: Bangladesh Haor and Wetland Development Board.
- Mitsch, W. J., & Gosselink, J. G. (2000). The value of wetlands: Importance of scale and landscape setting. *Ecological Economics*, 35(1), 25–33.
- Nagler, T., Rott, H., Ripper, E., Bippus, G., & Hetzenecker, M. (2016). Advancements for snowmelt monitoring by means of Sentinel-1 SAR. *Remote Sensing*, 8(4), 348.
- Ni, S., Chen, J., Wilson, C. R., & Hu, X. (2017). Long-term water storage changes of Lake Volta from grace and satellite altimetry and connections with regional climate. *Remote Sensing*, 9(8), 842.
- Ogawa, H., & Male, J. W. (1986). Simulating the flood mitigation role of wetlands. *Journal of Water Resources Planning and Management*, 112(1), 114–128. [https://doi.org/10.1061/\(asce\)0733-9496\(1986\)112:1\(114\)](https://doi.org/10.1061/(asce)0733-9496(1986)112:1(114))
- Pardo-Pascual, J. E., Almonacid-Caballer, J., Ruiz, L. A., & Palomar-Vázquez, J. (2012). Automatic extraction of shorelines from Landsat TM and ETM+ multi-temporal images with subpixel precision. *Remote Sensing of Environment*, 123, 1–11. <https://doi.org/10.1016/j.rse.2012.02.024>
- Parish, F. & Looi, C.C. (1999). Wetlands, biodiversity and climate change. In Options and needs for enhanced linkage between the Ramsar convention on wetlands, *Convention on Biological Diversity and UN Framework Convention on Climate Change*.
- Peng, D., Xiong, L., Guo, S., & Shu, N. (2005). Study of Dongting Lake area variation and its influence on water level using MODIS data/ Etude de la variation de la surface du Lac Dongting et de son influence sur le niveau d'eau, grâce à des données MODIS. *Hydrological Sciences Journal*, 50(1). <https://doi.org/10.1623/hysj.50.1.31.56327>
- Planet Imagery Product Specification (2019). Available online: https://www.planet.com/products/satelliteimagery/files/Planet_Combined_Imagery_Product_Specs_December2017.pdf
- Planet Team. (2017). Planet application program interface. In *Space for Life on Earth*. San Francisco, CA: Planet Team. Retrieved from <https://api.planet.com>
- Rosen, P., Hensley, S., Shaffer, S., Edelstein, W., Kim, Y., Kumar, R., et al. (2016). An update on the NASA-ISRO dual-frequency DBF SAR (NISAR) mission. In *2016 IEEE International Geoscience and Remote Sensing Symposium (IGARSS)* (pp. 2106–2108). IEEE.
- Rosen, P.A., Kim, Y., Kumar, R., Misra, T., Bhan, R. & Sagi, V. R. (2017). Global persistent SAR sampling with the NASA-ISRO SAR (NISAR) mission. In *2017 IEEE Radar Conference (RadarConf)* (pp. 0410–0414). IEEE.
- Shen, X., Wang, D., Mao, K., Anagnostou, E., & Hong, Y. (2019). Inundation extent mapping by synthetic aperture radar: A review. *Remote Sensing*, 11(7), 879.
- Smith, L. C., & Pavelsky, T. M. (2009). Remote sensing of volumetric storage changes in lakes. *Earth Surface Processes and Landforms*, 34(10), 1353–1358.
- Strobl, B., Etter, S., van Meerveld, I., & Seibert, J. (2019). The CrowdWater game: A playful way to improve the accuracy of crowdsourced water level class data. *PLoS ONE*, 14(9), e0222579. <https://doi.org/10.1371/journal.pone.0222579>
- Sulistioadi, Y. B., Tseng, K. H., Shum, C. K., Hidayat, H., Sumaryono, M., Suhardiman, A., et al. (2015). Satellite radar altimetry for monitoring small rivers and lakes in Indonesia. *Hydrology and Earth System Sciences*, 19(1), 341–359. <https://doi.org/10.5194/hess-19-341-2015>
- Thilsted, S. H. & Wahab, M. A. (2014). CGIAR research program on aquatic agricultural systems. Penang, Malaysia. Brochure: AAS-2014-07.
- Tong, X., Pan, H., Xie, H., Xu, X., Li, F., Chen, L., et al. (2016). Estimating water volume variations in Lake Victoria over the past 22 years using multi-mission altimetry and remotely sensed images. *Remote Sensing of Environment*, 187, 400–413.
- Turner, A. G., & Annamalai, H. (2012). Climate change and the South Asian summer monsoon. *Nature Climate Change*, 2(8), 587–595. <https://doi.org/10.1038/nclimate1495>
- Villadsen, H., Deng, X., Andersen, O. B., Stenseng, L., Nielsen, K., & Knudsen, P. (2016). Improved inland water levels from SAR altimetry using novel empirical and physical retracers. *Journal of Hydrology*, 537, 234–247.
- Wang, B. (2019). Monitoring inland surface water level from Sentinel-3 data (Master's thesis).
- White, L., Brisco, B., Daboor, M., Schmitt, A., & Pratt, A. (2015). A collection of SAR methodologies for monitoring wetlands. *Remote Sensing*, 7(6), 7615–7645.
- Wijesekara, G. N., Gupta, A., Valeo, C., Hasbani, J. G., Qiao, Y., Delaney, P., & Marceau, D. J. (2012). Assessing the impact of future land-use changes on hydrological processes in the Elbow River watershed in southern Alberta, Canada. *Journal of Hydrology*, 412, 220–232.
- Yang, J., & Zhang, J. (2019). Validation of Sentinel-3A/3B Satellite Altimetry Wave Heights with Buoy and Jason-3 Data. *Sensors*, 19(13), 2914. <https://doi.org/10.3390/s19132914>
- Yang, R., Zhu, L., Wang, J., Ju, J., Ma, Q., Turner, F., & Guo, Y. (2017). Spatiotemporal variations in volume of closed lakes on the Tibetan Plateau and their climatic responses from 1976 to 2013. *Climatic Change*, 140(3–4), 621–633.
- Yang, X., Zhao, S., Qin, X., Zhao, N., & Liang, L. (2017). Mapping of urban surface water bodies from Sentinel-2 MSI imagery at 10 m resolution via NDWI-based image sharpening. *Remote Sensing*, 9(6), 596.
- Zhao, W., Amelung, F., Doin, M. P., Dixon, T. H., Wdowinski, S., & Lin, G. (2016). InSAR observations of lake loading at Yangzhuoyong Lake, Tibet: Constraints on crustal elasticity. *Earth and Planetary Science Letters*, 449, 240–245.